

# Scaling Laws for Uncertainty in Deep Learning

**Mattia Rosso\***  
KAUST, Saudi Arabia

**Simone Rossi**  
EURECOM, France

**Giulio Franzese**  
EURECOM, France

**Markus Heinonen**  
Aalto University, Finland

**Maurizio Filippone**  
KAUST, Saudi Arabia

## Abstract

Deep learning has recently revealed the existence of scaling laws, demonstrating that model performance follows predictable trends based on dataset and model sizes. Inspired by these findings and fascinating phenomena emerging in the over-parameterized regime, we examine a parallel direction: do similar scaling laws govern predictive uncertainties in deep learning? In identifiable parametric models, such scaling laws can be derived in a straightforward manner by treating model parameters in a Bayesian way. In this case, for example, we obtain  $O(1/N)$  contraction rates for epistemic uncertainty with respect to the number of data  $N$ . However, in over-parameterized models, these guarantees do not hold, leading to largely unexplored behaviors.

In this work, we empirically show the existence of scaling laws associated with various measures of predictive uncertainty with respect to dataset and model sizes. Through experiments on vision and language tasks, we observe such scaling laws for in- and out-of-distribution predictive uncertainty estimated through popular approximate Bayesian inference and ensemble methods. Besides the elegance of scaling laws and the practical utility of extrapolating uncertainties to larger data or models, this work provides strong evidence to dispel recurring skepticism against Bayesian approaches: “*In many applications of deep learning we have so much data available: what do we need Bayes for?*” Our findings show that “*so much data*” is typically not enough to make epistemic uncertainty negligible.

## 1 Introduction

Deep learning has recently revealed empirical scaling laws: test performance tends to scale by a power-law  $f(x) \propto x^{-\gamma}$  of the size of the function, data or compute (Kaplan et al., 2020; Hoffmann et al., 2022). A related ‘double descent’ effect shows that increasing model capacity can surprisingly improve generalization (Belkin et al., 2019). These findings suggest that bigger models often perform better. A parallel question is: do similar scaling laws govern uncertainty in deep learning?

Bayesian deep learning provides a principled framework for quantifying uncertainty in neural networks by marginalizing weights, rather than

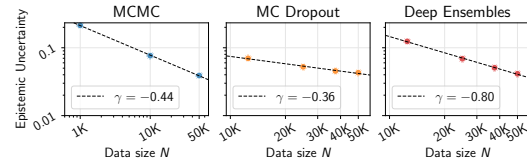


**Figure 1: Deep learning uncertainty is predictable, empirically.** ResNet-18 Epistemic Uncertainty scaling with the number of training data  $N$  on CIFAR-10.

\*Corresponding author: mattia.rosso@kaust.edu.sa

relying on point estimates, to obtain predictive uncertainties. (Neal, 1996; MacKay, 1995). Recent contributions show that, under rather simple conditions, inferring only a subset of model parameters can retain the capacity to represent any predictive distributions, at a significantly lower cost (Sharma et al., 2023)

The ability to produce well-calibrated predictive distributions and uncertainties is essential in decision-making and safety-critical applications, such as medical diagnosis and autonomous driving, where sound quantification of uncertainty can guide downstream choices (Papamarkou et al., 2024). However, exact Bayesian inference in large networks is intractable, which has motivated scalable approximations such as those based on the Laplace method (Ritter et al., 2018; Antoran et al., 2022), variational inference (Graves, 2011), Monte Carlo (MC) dropout (Gal and Ghahramani, 2016), along with (non-Bayesian) Deep Ensembles (Lakshminarayanan et al., 2017), which have proven effective and practical in obtaining sensible predictive uncertainties. Sampling-based methods, such as Stochastic Gradient Langevin Dynamics (SGLD) (Welling and Teh, 2011) and Stochastic Gradient Hamiltonian Monte Carlo (SGHMC) (Chen et al., 2014) provide scalable Markov chain Monte Carlo (MCMC) techniques for posterior inference over neural network weights. In the remainder of this paper, we will generally refer to Uncertainty Quantification (UQ) methods to indicate Bayesian and non-Bayesian approaches designed to obtain predictive uncertainties.

Despite recent criticism (Wimmer et al., 2023), current trends have focused on information-theoretic decomposition of predictive uncertainties into aleatoric and epistemic parts (Hüllermeier and Waegele, 2021). In this work, we study how *predictive uncertainties* evolves in deep models as training data size  $N$  grows. We evaluate a range of UQ methods and architectures for both vision and language modalities. We systematically vary optimization settings, prior choices, stochasticity level, and inference techniques. We demonstrate that different configurations exhibit a range of scaling behaviors across uncertainty metrics, but crucially all of them follow power-laws.

While classic results show  $O(1/N)$  posterior-variance contraction in identifiable parametric models (Cam, 1953), over-parameterized neural networks present challenges due to singular likelihoods, non-identifiability, and non-Gaussian posteriors. Although empirical scaling laws apply to test performance (Kaplan et al., 2020), a systematic understanding of how uncertainty scales with  $N$ , model size  $P$ , or optimization choices is lacking. Both Bayesian and non-Bayesian UQ approaches yield ensembles, where Epistemic Uncertainty (EU) quantifies ensemble diversity in predictions. We are particularly interested in determining when EU vanishes leading to ensemble collapse; this is where we can leverage the practical utility of scaling laws.

Several theories characterize neural networks in the large-data limit. Singular Learning Theory (SLT) models deep networks as singular statistical manifolds, claiming that singularities of loss minima determine learning behavior, and that generalization follows a power-law  $\mathcal{L} - \mathcal{L}_0 = \frac{\lambda}{n^\gamma}$  (Watanabe, 2009). Other perspectives include the manifold dimensionality hypothesis, linking generalization to the intrinsic dimensionality of learned representations (Ansini et al., 2019), and mechanistic interpretability efforts explaining simple scaling phenomena via emergent internal representations (Nanda et al., 2023). We derive a formal connection of generalization and total uncertainty in the case of linear models. We believe that such a framework may help to explain the scaling behavior of uncertainty in deep models.

In summary, our contributions are as follows:

- (i) *Empirical study.* We provide a comprehensive evaluation of predictive uncertainties using a variety of UQ methods across different architectures, modalities, and datasets. To the best of our knowledge, this is the first study to consider scaling laws associated with any form of uncertainty in deep learning.
- (ii) *Scaling patterns.* We empirically demonstrate that predictive uncertainties evaluated on in- and out-of-distribution, follow power-law trends with the dataset size. This allows us to extrapolate to large dataset sizes and to identify data regimes where UQ approaches remain relevant to characterize the diversity of the ensemble to a given numerical precision.
- (iii) *Theoretical insights.* We derive a formal connection between generalization error in SLT and total uncertainty in linear models. This novel analysis provides an interesting lead to explain the scaling laws observed in the experiments for over-parameterized models.

## 2 Background

### 2.1 Uncertainty Quantification

Predictive uncertainty refers to metrics associated with an ensemble of predictive distributions and it can be decomposed into Aleatoric Uncertainty (AU), arising from intrinsic data variability, and EU, reflecting uncertainty due to limited data or model knowledge (Hüllermeier and Waegeman, 2021).

The Total Uncertainty (TU) is the entropy of the mean predictive distribution

$$\text{TU}(\mathbf{x}) = \mathbb{H} \left[ \frac{1}{K} \sum_{k=1}^K p(y|\mathbf{x}, \boldsymbol{\theta}^{(k)}) \right], \quad (1)$$

where  $\boldsymbol{\theta}^{(k)}$  are the model parameters of the  $k$ 'th ensemble member or stochastic pass, and  $p(y|\mathbf{x}, \boldsymbol{\theta}^{(k)})$  is its predictive distribution. The irreducible uncertainty AU is the average entropy of predictions:

$$\text{AU}(\mathbf{x}) = \frac{1}{K} \sum_{k=1}^K \mathbb{H} \left[ p(y|\mathbf{x}, \boldsymbol{\theta}^{(k)}) \right]. \quad (2)$$

Finally, the reducible uncertainty EU is their difference,

$$\text{EU}(\mathbf{x}) = \text{TU}(\mathbf{x}) - \text{AU}(\mathbf{x}). \quad (3)$$

In this work we study the power-law of test predictive uncertainty against training size  $N$ ,

$$\frac{1}{N_{\text{test}}} \sum_{n=1}^{N_{\text{test}}} \text{Unc}(\mathbf{x}_n), \quad \text{Unc} \in \{\text{TU}, \text{AU}, \text{EU}\}. \quad (4)$$

While popular, these entropy-based metrics have limitations: (i) The standard decomposition of TU assumes additive separation of AU and EU, which Wimmer et al. (2023) argues not to hold in complex deep models, and the difficulty of disentangling them hinders their interpretability (de Jong et al., 2024); (ii) Recent works highlight epistemic uncertainty collapse of large ensembles, leading to overly confident predictions (Kirsch, 2024; Fellaji and Pennerath, 2024).

Despite these criticisms, these metrics remain useful and tractable in practice, especially when paired with typical UQ methods. Their consistency across tasks such as active learning, out-of-distribution detection and model calibration makes them valuable diagnostic tools.

### 2.2 Scaling Laws and Generalization

Empirical studies in deep learning have demonstrated that performance metrics scale predictably in model size, dataset size and compute. Initial findings by Hestness et al. (2017) and Kaplan et al. (2020) showed that test loss typically decreases following a power-law of the form

$$\mathcal{L}(x) = \mathcal{L}_{\infty} + \left( \frac{x_0}{x} \right)^{\alpha}, \quad (5)$$

where  $x$  is the resource under analysis (e.g., dataset size  $N$ , model size  $P$ , or compute budget  $C$ ),  $\mathcal{L}_{\infty}$  is the irreducible loss, and  $\alpha$  is modality- and task-specific ( $x_0$  is a reference constant). These relationships hold consistently across model architectures, tasks, and modalities, as empirically shown by Henighan et al. (2020), who demonstrated similar loss scaling for language, image, video and multimodal domains. The scaling exponents differ across domains, but the functional form of the scaling law remains stable, indicating a general underlying behavior.

Theoretical explanations of scaling behaviors are only recently emerging: for example Sharma and Kaplan (2022); Bahri et al. (2024) linked  $\alpha$  to the intrinsic dimension and spectral properties of the data, showing how the data geometry drives the reducible portion of the loss. However, despite these empirical and theoretical advances, a comprehensive understanding of how epistemic and aleatoric uncertainties scales with model and data size remain an open question. Indeed, a Bayesian perspective on uncertainty scaling laws is currently missing: it is unclear what kind of power laws uncertainty exhibits, if any. Understanding uncertainty scaling could significantly enhance the development and comprehension of Bayesian deep learning.

### 3 Methods

In this section, we describe the approximate Bayesian inference and ensemble methods used in our experiments. We hypothesize that if uncertainty scaling laws exist, they should emerge regardless of the UQ method.

**MC Dropout.** MC dropout is a simple and common inference method, with connections to variational inference (Gal and Ghahramani, 2016). During training standard dropout is applied, while at test time dropout masks are resampled to produce stochastic forward passes, yielding ensemble predictions. Due to its simplicity and universality, MC dropout is a good UQ baseline.

**Gaussian Approximations.** Gaussian are a common family of posterior approximations, and include Laplace approximations (Ritter et al., 2018) and Variational Inference (Graves, 2011). In Laplace approximations the curvature of the log-posterior at a local optimum determines the covariance of the Gaussian approximation. In variational inference, the optimization seeks an approximate distribution close to the true posterior in the Kullback-Leibler divergence (KL) sense.

**Markov Chain Monte Carlo.** MCMC is the classic method of obtaining samples from the posterior over model parameters (Neal, 1996; MacKay, 1995). Gradient-based MCMC, such as Hamiltonian Monte Carlo, are some of the most effective samplers. Mini-batch-based SGHMC (Chen et al., 2014) and Langevin dynamics (Welling and Teh, 2011) have been successfully proposed to sample from the posterior over parameters of deep neural networks of moderate size (Tran et al., 2022; Izmailov et al., 2021). We consider parameter sampling with both global parameter priors and Gaussian process functional priors (Tran et al., 2022).

**Deep Ensembles.** Deep ensembles (Lakshminarayanan et al., 2017) are a popular technique to obtain predictive uncertainties, despite lacking a full Bayesian interpretation. Multiple networks are trained independently from different seeds and uncertainty is estimated from the ensemble of predictions. Deep ensembles tend to provide better uncertainty estimates and are more robust to model misspecification than MC dropout. We train ensembles of size  $M \in \{5, 10\}$ .

**Partially stochastic networks.** We consider partially stochastic networks where only few layers are inferred, while rest are optimized in a standard way (Sharma et al., 2023).

## 4 Experiments

In this section, we present a detailed analysis of the extensive experimental results from our study. We begin by focusing on the most significant findings in the vision domain, highlighting the scaling behaviors of uncertainty both in- and out-of-distribution. Additionally, we report on an additional experiment conducted in the text classification setting with a GPT-2 language model. Our investigation spans a wide matrix of experimental configurations, aiming to explore a broad range of combinations across architectures, datasets and UQ setups.

### 4.1 Image classification

We use common image classification architectures of ResNet (He et al., 2016), WideResNet (Zagoruyko and Komodakis, 2016) and Vision Transformer (ViT) (Dosovitskiy et al., 2021). We report CIFAR-10 and ImageNet32 results in the main paper, and results on CIFAR-100 in Appendix B.

#### 4.1.1 ResNet and WideResNet architectures

If not specified, we train these models for 400 epochs with SGD optimizer (momentum 0.9 and weight decay  $5 \times 10^{-4}$ ); in some experiments we adopt a cosine annealing scheduler on the learning rate and in others we do not. See Appendix C for more experimental details.

In ResNets, we add dropout layers after the convolutional blocks and before the fully connected layers following Kim et al. (2023). For WideResNets, we adopt the official implementation by Zagoruyko and Komodakis (2016), where dropout is applied between the two convolutional layers within each

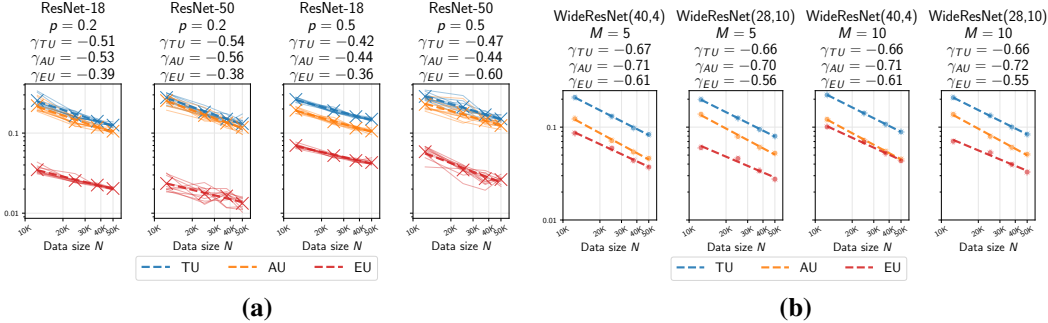


Figure 2: **ResNet and WideResNet(w-d) uncertainty scaling on CIFAR-10 dataset:** In (a) we use MC dropout with fixed dropout rate  $p = 0.2$  and  $p = 0.5$ . In (b) we use Deep Ensembles (with  $M = 5$  and  $M = 10$  ensemble members). We consider 25%, 50%, 75% and 100% subsets of the training data. In (a), each point  $\times$  corresponds to the average over 10 independent folds (varying both data subsampling and model initialization), whereas in (b), the results for WideResNets are reported from a single fold. Dashed lines represent linear regressions fitted to the mean uncertainty metrics (AU, EU, TU) on a fixed test set (see Section 2.1), following a power-law decay of the form  $1/N^{\gamma_{TU}}$ ,  $1/N^{\gamma_{AU}}$ , and  $1/N^{\gamma_{EU}}$ . Both axes are shown on a logarithmic scale.

residual unit. We experiment with various dropout rates finding more expressivity in the scaling laws obtained with  $p = 0.5$ , especially in ResNets architectures (Gal et al., 2017). Some results are reported in Fig. 2 and Fig. 7. Furthermore, we examine the impact of combining MC dropout with Sharpness Aware Minimization (SAM) (Foret et al., 2020) to investigate how two techniques that independently improve generalization interact in terms of uncertainty. Our intuition behind the increasing trend of EU in Fig. 3 is that SAM seeks to minimize a perturbed loss objective that penalizes sharp minima in the loss landscape. As dataset size increases, the curvature of the loss function (as measured by the spectral properties of the Hessian) increases. SAM, which aims to avoid sharp valleys in the loss landscape, is therefore forced to navigate an increasingly curved landscape as  $N \rightarrow \infty$ . If the optimizer selects flatter basins in response to this increased curvature, it may avoid parameter regions that would otherwise exhibit low epistemic variance, and instead, it may prefer broader, flatter regions that span a more diverse set of functions—yielding higher epistemic uncertainty.

Across our experiments, we observe that the EU is typically smaller than the AU. Finally, we report results training on CIFAR-10 and testing on CIFAR-10-C (corrupted), which allows us to explore how uncertainty behaves out-of-distribution (OOD); results in Fig. 6.

In Fig. 2, we report scaling laws for Deep Ensembles (Lakshminarayanan et al., 2017), using  $M = 5$  and  $M = 10$  independently trained models. Even for this UQ approach, we observe the emergence of power-law scalings of uncertainties with respect to the number of data.

We also observe a similar behavior for MCMC. In these experiments, we choose a weakly informative prior over all parameters with zero mean and standard deviation of 10. In Appendix B, we also report results for MCMC after optimizing the priors according to the approach in Tran et al. (2022), where we target a Gaussian process (GP) with isotropic covariance with log-length-scale of  $\frac{1}{2} \log D$  and log-marginal variance of 2. In Fig. 8 MCMC (1) and MCMC (2) refer to the approach of treating the first and first+second layers of the model in a stochastic fashion, while the other parameters are kept fixed to a pretrained solution.

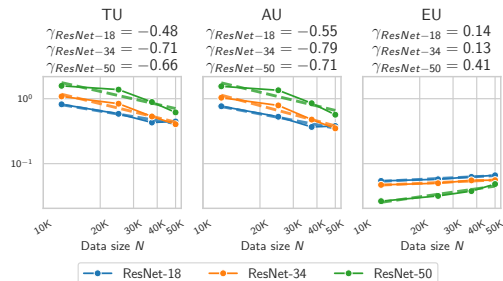
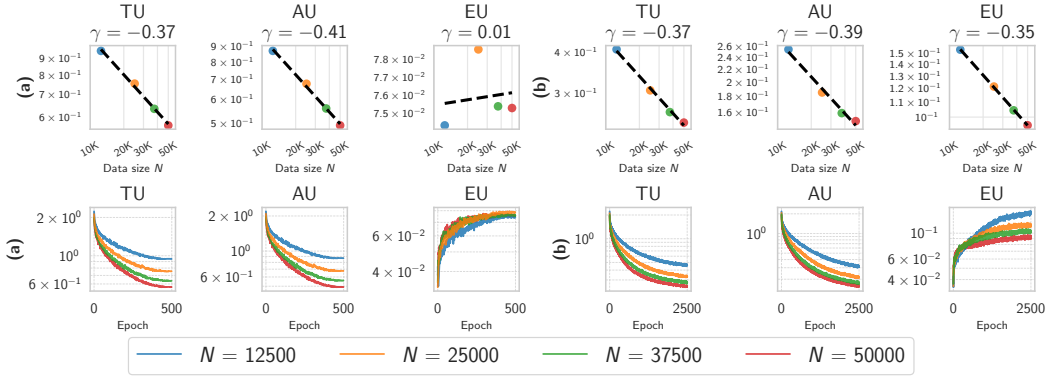


Figure 3: **Impact of SGD+SAM on uncertainty scaling:** ResNets on CIFAR-10 dataset - MC dropout ( $p = 0.5$ ).



**Figure 5: ViT-small uncertainty training dynamics on CIFAR-10 dataset:** In (a) we use MC dropout ( $p = 0.5$ ) and we train the model for 500 epochs with Adam optimizer (Kingma and Ba, 2017) and cosine annealing. In (b) we train the same model for 2500 epochs and fixed learning rate  $10^{-4}$ . The training dynamics show that the shape/speed of convergence of of TU, AU, EU strongly depends on the optimization trajectories underneath.

#### 4.1.2 Vision Transformer

We explore uncertainty scaling trends using Vision Transformer (ViT) architectures (Dosovitskiy et al., 2021). We use a compact ViT model trained on both CIFAR-10 and ImageNet32. The architecture consists of a 6-layer transformer with 8 attention heads per layer and input images are tokenized in 4 patches. We apply MC dropout with a fixed rate of 0.5 both on the embeddings and in the transformer blocks. We conduct an ablation study in Fig. 5 to highlight how different experimental settings lead to completely different uncertainty behaviors.

It is interesting to observe the effect of the cosine annealing learning schedule, also visible in Fig. 5 when training on CIFAR-10, suggesting that early-phase uncertainty dynamics in transformers can be sensitive to optimization strategies. Results on ImageNet32 are reported in Appendix B .

#### 4.2 Text classification

We further investigate the language modality by assessing uncertainty estimates on the pre-trained Phi-2 model (Abdin et al., 2024), applying a Laplace approximation to the posterior over the LoRA parameters (Yang et al., 2024). We fine-tuned the model on qqp and ARC datasets observing that the uncertainties remained flat for every data subset used for fine tuning (see Fig. 15). This saturation effect is likely due to the massive dataset used for pre-training, limiting the expressiveness of the model uncertainty on comparatively much smaller data for fine tuning.

##### 4.2.1 GPT-2 on Algorithmic Dataset

We train a GPT-2 model to solve modular arithmetic problems from a synthetic dataset based on the setup in Power et al. (2022). The model learns to predict the token following the equals sign. We only experiment with MC dropout with rate 0.1 to estimate predictive uncertainty. Interestingly, more evident uncertainty scaling patterns only emerge after extensive training, suggesting potential links between grokking dynamics (Belkin et al., 2019) and uncertainty behavior. In Fig. 4 we show predictive uncertainties when training the model on increasing percentages (from 5% to 90%) of the MODULO 97 algorithmic dataset.

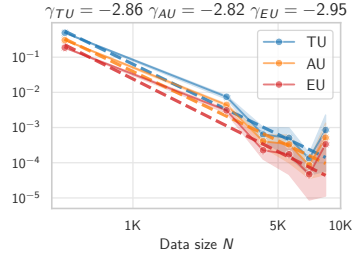


**Figure 4: Algorithmic dataset:** GPT-2 model on the Algorithmic Dataset to learn the modulo addition operation. Results obtained by training for 10 000 epochs averaged over 3 folds.

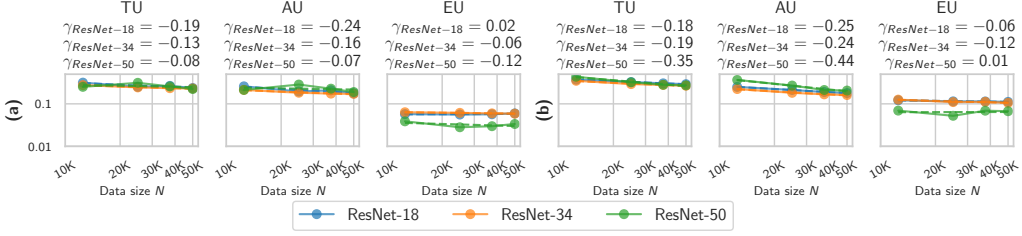


Figure 6: **ResNets on CIFAR10-C dataset:** MC dropout with  $p = 0.2$  in **(a)** and  $p = 0.5$  in **(b)**. For models trained on incrementally larger training subsets of CIFAR-10, we report the predictive uncertainties when testing on the (whole) CIFAR10-C dataset, averaged over all corruption levels (1-5) and corruption types considered.

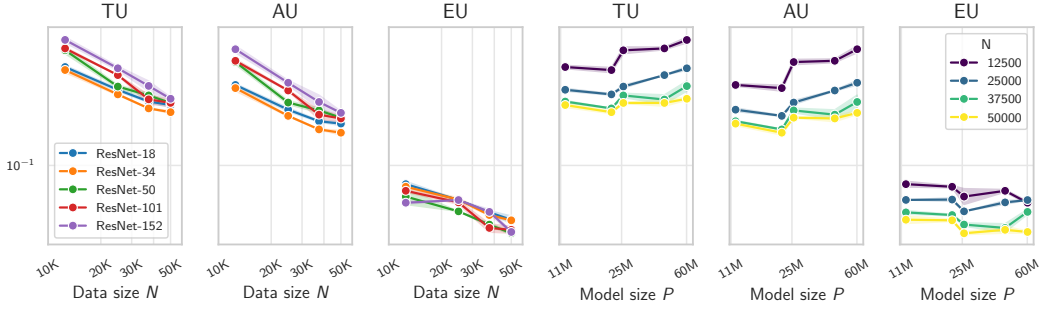


Figure 7: **Uncertainty scaling with model parameters:** An extensive range of ResNets architectures on CIFAR-10 dataset - MC dropout ( $p = 0.5$ ). We train all these architectures for 400 epochs and fixed learning rate  $10^{-3}$ .

## 5 Theoretical connections

The theory of identifiable models has extensively analyzed asymptotic behaviors, such as posterior contraction and convergence of test loss and generalization error. In this section, we recall how predictive uncertainty contracts with increasing data in Bayesian linear regression, highlight its connection to Watanabe’s Generalization Error, and outline links to Singular Learning Theory.

### 5.1 TU scaling in Identifiable Parametric Models

We consider Bayesian linear regression  $y = \boldsymbol{\theta}^\top \phi(\mathbf{x}) + \epsilon$ , where  $\boldsymbol{\theta} \in \mathbb{R}^P$  are parameters of interest, and  $\phi(\mathbf{x}) = [\phi_1(\mathbf{x}), \phi_2(\mathbf{x}), \dots, \phi_P(\mathbf{x})]^\top$  are the basis functions, and assume zero-mean noise  $\epsilon \sim \mathcal{N}(0, \sigma^2)$ . We define the likelihood over  $N$  iid observations  $\{\mathbf{X}, \mathbf{y}\} = \{(\mathbf{x}_i, y_i)\}_{i=1}^N$ ,

$$p(\mathbf{y}|\mathbf{X}, \boldsymbol{\theta}, \sigma^2) = \prod_{n=1}^N \mathcal{N}(y_n | \phi(\mathbf{x}_n)^\top \boldsymbol{\theta}, \sigma^2). \quad (6)$$

By assuming a conjugate Gaussian prior  $p(\boldsymbol{\theta}) = \mathcal{N}(\boldsymbol{\theta} | \mathbf{m}_0, \mathbf{S}_0)$  the posterior is also Gaussian with mean  $\mathbf{m}_N = \mathbf{S}_N^{-1} \mathbf{m}_0 + \sigma^{-2} \Phi^\top \mathbf{y}$  and covariance  $\mathbf{S}_N = (\sigma^{-2} \Phi^\top \Phi + \mathbf{S}_0^{-1})^{-1}$ . The predictive posterior for a new test points  $(\mathbf{x}_*, y_*)$  is also Gaussian,  $p(y_* | \mathbf{x}_*, \mathbf{y}, \mathbf{X}) = \mathcal{N}(y_* | \mathbf{m}_N^\top \phi(\mathbf{x}_*), \sigma_N^2(\mathbf{x}_*))$  with  $\sigma_N^2(\mathbf{x}_*) = \sigma^2 + \phi(\mathbf{x}_*)^\top \mathbf{S}_N \phi(\mathbf{x}_*)$ .

The predictive variance  $\text{Var}[y_* | \mathbf{x}_*, \mathbf{y}, \mathbf{X}]$  decomposes into the uncertainty of data  $\sigma^2$  (AU), and the uncertainty of parameters  $\phi(\mathbf{x}_*)^\top \mathbf{S}_N \phi(\mathbf{x}_*)$  (EU). We stress that EU is made available only by taking the Bayesian approach of treating  $\boldsymbol{\theta}$  as a random variable. It can be shown that  $\sigma_{N+1}^2(\mathbf{x}_*) \leq \sigma_N^2(\mathbf{x}_*)$

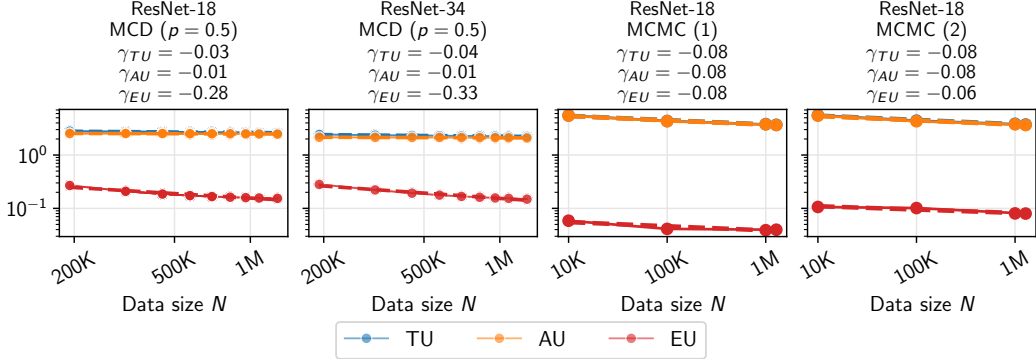


Figure 8: **Uncertainty estimates for ResNets on ImageNet-32 dataset:** The first two subplots report MC dropout ( $p = 0.5$ ) uncertainties for ResNet-18 and ResNet-34, trained with fixed learning rate  $10^{-3}$  on 9 increasing subsets of the training data. We also report uncertainties obtained through MCMC considering only the first layer stochastic (MCMC (1)) and only the first two layers stochastic (MCMC (2)) for ResNet-18 trained on 4 increasing subsets of the training data.

– the posterior distribution becomes narrower as additional data points are observed (Qazaz et al., 1997). Moreover, in the limit of  $N \rightarrow \infty$  we get  $\sigma_N^2(\mathbf{x}) \rightarrow \sigma^2$ : in the infinite data regime, the predictive uncertainty converges to its irreducible AU component.

## 5.2 Singular Learning Theory

Our speculative theoretical link is SLT, which provides insights into the learning dynamics of highly overparameterized models. The Fisher information of deep neural networks is often singular at certain parameter values; despite forming a measure-zero subset, these singularities significantly influence learning. SLT proves that the asymptotic properties of learning are shaped by the geometry near such degenerate points (Watanabe, 2009, 2018). One main quantity of interest in this framework is the generalization error  $G$ . Here we limit ourself to connect this to the TU in Bayesian Linear Regression. Using Watanabe’s notation

$$F_N = -\log p(\mathbf{y}_N | \mathbf{X}_N) = -\log \int p(\mathbf{y}_N | \mathbf{X}_N, \boldsymbol{\theta}) p(\boldsymbol{\theta}) d\boldsymbol{\theta} \quad (7)$$

is the negative marginal log likelihood (NMLL) of the data  $\mathbf{X}_N$  of size  $N$ . The generalization error  $G_N = \mathbb{E}_{p(y_{N+1} | \mathbf{x}_{N+1}, \hat{\boldsymbol{\theta}})} [F_{N+1}] - F_N$  measures the expected increase in marginal likelihood when training with one additional data point (See Appendix A.2) and it can be rewritten as:

$$G_N = -\underbrace{\mathbb{E}_{p(y_{N+1} | \mathbf{x}_{N+1}, \boldsymbol{\theta})}}_{p(y)} \left[ \log \underbrace{p(y_{N+1} | \mathbf{x}_{N+1}, \mathbf{X}_N, \mathbf{y}_N)}_{q_N(y)} \right], \quad (8)$$

which reduces to the log posterior predictive distribution for the  $(N + 1)$ ’th datapoint given the first  $N$  datapoints, under the true process

$$y_{N+1} \sim \mathcal{N}(y_{N+1} | \boldsymbol{\theta}_{\text{true}}^\top \mathbf{x}_{N+1}, \sigma_{\text{true}}^2). \quad (9)$$

By denoting the true process by  $p(y)$  and the posterior predictive from  $N$  data by  $q_N(y)$  we can manipulate the expression of the generalization error to obtain:

$$G_N = -\underbrace{\frac{1}{2} \log(2\pi e \sigma_{\text{true}}^2)}_{\text{aleatoric uncertainty}} - \underbrace{\text{KL}[p(y) || q_N(y)]}_{\text{epistemic uncertainty}}, \quad (10)$$

where  $\text{KL}[p(y) || q_N(y)]$  is the KL divergence between the true and the posterior predictive distribution, quantifying the epistemic uncertainty arising from limited knowledge of the true model parameters.

By looking at the asymptotic expression of TU as  $N \rightarrow \infty$  and by taking, without loss of generality, identity basis functions, we get:

$$\text{TU}(\mathbf{x}_{N+1}) = \mathbb{H}[q_N(y)] \quad (11)$$

$$= \frac{1}{2} \log(2\pi e \sigma_{\text{true}}^2) + \frac{1}{2(N+1)} \mathbf{x}_{N+1}^\top \boldsymbol{\Sigma}_{X_{N+1}}^{-1} \mathbf{x}_{N+1} + O\left(\frac{1}{(N+1)^2}\right). \quad (12)$$

As more data is collected, the predictive posterior  $q_N(y)$  converges toward the true predictive distribution  $p(y)$ . Consequently, the generalization error  $G_N$  asymptotically approaches the irreducible aleatoric uncertainty. Similarly, the TU converges to the aleatoric component as the epistemic part vanishes. In [Watanabe \(1999\)](#) it's proved an asymptotic expansion of  $G_N$  which is proportional to the effective dimensionality of the model.

We hypothesize that the theoretical tools provided by this framework, closely linked to concepts from Statistical Physics, may offer a promising foundation to explain some of the scaling behaviors we have observed. In particular, we find recent efforts to computationally characterize the effective dimensionality of deep learning models especially compelling ([Lau et al., 2024](#); [Chen et al., 2024](#)), and we aim to investigate formal connections in future extensions of this work.

## 6 Conclusions

Inspired by recent works on scaling laws in deep learning, we investigated whether these apply to predictive uncertainties as well. Our empirical findings on computer vision and language tasks indicate that these scaling laws appear in a broad range of design choices, including architecture design, posterior approximation/ensembling approach, and hyper-parameters.

We set out to explain the emergence of such scaling laws and, inspired by SLT, we provide novel theoretical insights on the connections between generalization error and predictive uncertainty. This helps us in understanding the power-law behavior associated with the scaling of information-theoretic measures of uncertainty with respect to dataset size.

While the theory gives some indications along these lines, the experiments reveal that obtaining exact power-law coefficients from the theory is not easy, as choices of model architecture, UQ method, and hyper-parameters affect such coefficients in unpredictable ways. As a result, we believe that our work can be used to derive practical strategies to extrapolate uncertainties to large  $N$ , e.g., to predict how much data is needed to obtain ensemble predictions which are indistinguishable up to a given numerical precision.

In future works, we will investigate alternative theoretical angles to explain scaling laws on uncertainties in deep learning. One approach could be to study the behavior of uncertainties in models with large number of units, such as WideResNets, and connect their uncertainties with those obtained by Gaussian processes .

**Limitations** Previous works on scaling laws for deep learning show clear trends of test performance with respect to model parameters; however, with our experimental setup, we did not observe the same for predictive uncertainties (see [Fig. 7](#)) and we were hoping to have more computational resources to investigate this aspect in more detail. Another element characterizing scaling laws for test performance is the behavior with respect to computational budget, which we do not consider here, again for reasons related to limited computational resources. Finally, it would have been great to study more applications where we could test the extrapolation of scaling laws to very large dataset sizes, in addition to the experiments on the GPT-2 language model.

**Broader impacts.** This paper demonstrates the emergence of scaling laws of uncertainties in deep learning. The results should motivate a wider adoption of UQ methods for deep learning, even in the case of supposedly large datasets, in order to obtain uncertainties that can be used to assist decision-making.

## References

- M. I. Abdin et al. Phi-3 technical report: A highly capable language model locally on your phone. Technical Report MSR-TR-2024-12, Microsoft, August 2024.
- A. Ansuini, A. Laio, J. Macke, and D. Zoccolan. Intrinsic dimension of data representations in deep neural networks. In *Advances in Neural Information Processing Systems*, 2019.
- J. Antoran, D. Janz, J. U. Allingham, E. Daxberger, R. R. Barbano, E. Nalisnick, and J. M. Hernandez-Lobato. Adapting the linearised Laplace model evidence for modern deep learning. In *International Conference on Machine Learning*, 2022.
- Y. Bahri, E. Dyer, J. Kaplan, J. Lee, and U. Sharma. Explaining neural scaling laws. *Proceedings of the National Academy of Sciences*, 121(27):e2311878121, 2024.
- M. Belkin, D. Hsu, S. Ma, and S. Mandal. Reconciling modern machine-learning practice and the classical bias–variance trade-off. *Proceedings of the National Academy of Sciences*, 2019.
- L. Cam. *On Some Asymptotic Properties of Maximum Likelihood Estimates and Related Bayes' Estimates*. University of California Press, 1953.
- D. Chen, W.-K. Chang, and P. Chaudhari. Learning capacity: A measure of the effective dimensionality of a model. *arXiv*, 2024.
- T. Chen, E. Fox, and C. Guestrin. Stochastic gradient Hamiltonian Monte Carlo. In *International Conference on Machine Learning*, 2014.
- I. P. de Jong, A. I. Sburlea, and M. Valdenegro-Toro. How disentangled are your classification uncertainties? *arXiv*, 2024.
- A. Dosovitskiy, L. Beyer, A. Kolesnikov, D. Weissenborn, X. Zhai, T. Unterthiner, M. Dehghani, M. Minderer, G. Heigold, S. Gelly, J. Uszkoreit, and N. Houlsby. An image is worth 16x16 words: Transformers for image recognition at scale. In *International Conference on Learning Representations*, 2021.
- M. Fellaji and F. Pennerath. The epistemic uncertainty hole: An issue of Bayesian neural networks. *arXiv*, 2024.
- P. Foret, A. Kleiner, H. Mobahi, and B. Neyshabur. Sharpness-aware minimization for efficiently improving generalization. *arXiv*, 2020.
- Y. Gal and Z. Ghahramani. Dropout as a Bayesian approximation: Representing model uncertainty in deep learning. In *International Conference on Machine Learning*, 2016.
- Y. Gal, J. Hron, and A. Kendall. Concrete dropout. In *Advances in Neural Information Processing Systems*, 2017.
- A. Graves. Practical variational inference for neural networks. In *Advances in Neural Information Processing Systems*, 2011.
- N. Hayashi and Y. Sawada. Bayesian generalization error in linear neural networks with concept bottleneck structure and multitask formulation. *Neurocomputing*, 638:130165, 2025.
- K. He, X. Zhang, S. Ren, and J. Sun. Deep residual learning for image recognition. *IEEE Conference on Computer Vision and Pattern Recognition*, 2016.
- T. Henighan, J. Kaplan, M. Katz, M. Chen, C. Hesse, J. Jackson, H. Jun, T. B. Brown, P. Dhariwal, S. Gray, C. Hallacy, B. Mann, A. Radford, A. Ramesh, N. Ryder, D. M. Ziegler, J. Schulman, D. Amodei, and S. McCandlish. Scaling laws for autoregressive generative modeling. *arXiv*, 2020.
- J. Hestness, S. Narang, N. Ardalani, G. F. Diamos, H. Jun, H. Kianinejad, M. A. Patwary, Y. Yang, and Y. Zhou. Deep learning scaling is predictable, empirically. *ArXiv*, 2017.

- J. Hoffmann, S. Borgeaud, A. Mensch, E. Buchatskaya, T. Cai, E. Rutherford, D. de Las Casas, L. A. Hendricks, J. Welbl, A. Clark, T. Hennigan, E. Noland, K. Millican, G. van den Driessche, B. Damoc, A. Guy, S. Osindero, K. Simonyan, E. Elsen, O. Vinyals, J. W. Rae, and L. Sifre. Training compute-optimal large language models. In *NeurIPS*, 2022.
- E. Hüllermeier and W. Waegeman. Aleatoric and epistemic uncertainty in machine learning: an introduction to concepts and methods. *Machine Learning*, 2021.
- P. Izmailov, S. Vikram, M. D. Hoffman, and A. G. G. Wilson. What are Bayesian neural network posteriors really like? In *International conference on machine learning*, pages 4629–4640. PMLR, 2021.
- J. Kaplan, S. McCandlish, T. Henighan, T. B. Brown, B. Chess, R. Child, S. Gray, A. Radford, J. Wu, and D. Amodei. Scaling laws for neural language models. *ArXiv*, 2020.
- B. J. Kim, H. Choi, H. Jang, D. Lee, and S. W. Kim. How to use dropout correctly on residual networks with batch normalization. In *Conference on Uncertainty in Artificial Intelligence*, 2023.
- D. P. Kingma and J. Ba. Adam: A method for stochastic optimization, 2017.
- A. Kirsch. (implicit) ensembles of ensembles: Epistemic uncertainty collapse in large models. In *NeurIPS 2024 Workshop on Bayesian Decision-making and Uncertainty*, 2024.
- B. Lakshminarayanan, A. Pritzel, and C. Blundell. Simple and scalable predictive uncertainty estimation using deep ensembles. In *Advances in Neural Information Processing Systems*, 2017.
- E. Lau, Z. Furman, G. Wang, D. Murfet, and S. Wei. The local learning coefficient: A singularity-aware complexity measure. *arXiv*, 2024.
- D. J. MacKay. Bayesian neural networks and density networks. *Nuclear Instruments and Methods in Physics Research Section A*, 354(1):73–80, 1995.
- N. Nanda, L. Chan, T. Lieberum, J. Smith, and J. Steinhardt. Progress measures for grokking via mechanistic interpretability. *arXiv*, 2023.
- R. Neal. *Bayesian Learning for Neural Networks*. Springer-Verlag, 1996.
- T. Papamarkou, M. Skoulios, K. Palla, L. Aitchison, J. Arbel, D. Dunson, M. Filippone, V. Fortuin, P. Hennig, J. M. Hernández-Lobato, A. Hubin, A. Immer, T. Karaletsos, M. E. Khan, A. Kristiadi, Y. Li, S. Mandt, C. Nemeth, M. A. Osborne, T. G. J. Rudner, D. Rügamer, Y. W. Teh, M. Welling, A. G. Wilson, and R. Zhang. Position: Bayesian deep learning is needed in the age of large-scale AI. In *International Conference on Machine Learning*, 2024.
- A. Power, Y. Burda, H. Edwards, I. Babuschkin, and V. Misra. Grokking: Generalization beyond overfitting on small algorithmic datasets. *arXiv*, 2022.
- C. S. Qazaz, C. K. I. Williams, and C. M. Bishop. An upper bound on the Bayesian error bars for generalized linear regression. In *Proceedings of the First International Conference on Mathematics of Neural Networks*, 1997.
- H. Ritter, A. Botev, and D. Barber. A scalable Laplace approximation for neural networks. In *International conference on learning representations*, 2018.
- M. Sharma, S. Farquhar, E. Nalisnick, and T. Rainforth. Do Bayesian neural networks need to be fully stochastic? In *International Conference on Artificial Intelligence and Statistics*, 2023.
- U. Sharma and J. Kaplan. Scaling laws from the data manifold dimension. *Journal of Machine Learning Research*, 23(9):1–34, 2022.
- B.-H. Tran, S. Rossi, D. Miliros, and M. Filippone. All you need is a good functional prior for Bayesian deep learning. *Journal of Machine Learning Research*, 2022.
- S. Watanabe. Algebraic analysis for non-regular learning machines. In *Advances in Neural Information Processing Systems*, 1999.

- S. Watanabe. *Algebraic Geometry and Statistical Learning Theory*. Cambridge University Press, 2009.
- S. Watanabe. *Mathematical Theory of Bayesian Statistics*. CRC Press, Taylor & Francis Group, 2018.
- M. Welling and Y. W. Teh. Bayesian learning via stochastic gradient Langevin dynamics. In *International Conference on International Conference on Machine Learning*, 2011.
- L. Wimmer, Y. Sale, P. Hofman, B. Bischl, and E. Hüllermeier. Quantifying aleatoric and epistemic uncertainty in machine learning: Are conditional entropy and mutual information appropriate measures? In *Conference on Uncertainty in Artificial Intelligence*, 2023.
- A. Yang, M. Robeyns, X. Wang, and L. Aitchison. Bayesian low-rank adaptation for large language models. 2024.
- S. Zagoruyko and N. Komodakis. Wide residual networks. *arXiv*, 2016.

## A Appendix

### A.1 Total Uncertainty in Bayesian Linear Regression

We consider a class of models defined as a linear combination of fixed nonlinear functions of the input variables of the form:

$$y(\mathbf{x}, \boldsymbol{\theta}) = \sum_{j=0}^{M-1} \theta_j \phi_j(\mathbf{x}) = \boldsymbol{\theta}^\top \boldsymbol{\phi}(\mathbf{x}), \quad (13)$$

where  $\boldsymbol{\theta} = (\theta_0, \dots, \theta_{M-1})^\top$  are model parameters and  $\boldsymbol{\phi} = (\phi_0, \dots, \phi_{M-1})^\top$  are known as *basis functions* which allow  $y(\mathbf{x}, \boldsymbol{\theta})$  to be a non-linear function of the input  $\mathbf{x}$ .

We consider the target variable  $y$  that is given by a deterministic function  $y(\mathbf{x}, \boldsymbol{\theta})$  plus additive Gaussian noise:

$$y = \boldsymbol{\theta}^\top \boldsymbol{\phi}(\mathbf{x}) + \epsilon, \quad (14)$$

where  $\boldsymbol{\theta}$  is treated as a random vector and  $\epsilon \sim \mathcal{N}(0, \sigma^2)$ , obtaining

$$p(y|\mathbf{x}, \boldsymbol{\theta}, \sigma^2) = \mathcal{N}(y|\boldsymbol{\phi}(\mathbf{x})^\top \boldsymbol{\theta}, \sigma^2). \quad (15)$$

We consider a supervised learning problem with  $N$  input-label training pairs  $\{\mathbf{X}, \mathbf{y}\} = \{(\mathbf{x}_i, y_i)\}_{i=1}^N$ . Assuming that the data points are drawn independently from Eq. (15), the likelihood becomes:

$$p(\mathbf{y}|\mathbf{X}, \boldsymbol{\theta}, \sigma^2) = \prod_{n=1}^N \mathcal{N}(y_n|\boldsymbol{\phi}(\mathbf{x}_n)^\top \boldsymbol{\theta}, \sigma^2). \quad (16)$$

According to the transformation of the features introduced by the set of basis functions  $\boldsymbol{\phi}$ , we define the design matrix  $\Phi \in \mathbb{R}^{N \times M}$  with entries  $\Phi_{nj} = \phi_j(\mathbf{x}_n)$ . We assume a conjugate prior over  $\boldsymbol{\theta}$ :

$$p(\boldsymbol{\theta}) = \mathcal{N}(\boldsymbol{\theta}|\boldsymbol{\mu}_0, \boldsymbol{\Sigma}_0). \quad (17)$$

From Bayes' theorem, the posterior can be derived in closed form leading to the following result:

$$p(\boldsymbol{\theta}|\mathbf{y}, \mathbf{X}) = \mathcal{N}(\boldsymbol{\theta}|\boldsymbol{\mu}_N, \boldsymbol{\Sigma}_N), \quad (18)$$

$$\boldsymbol{\mu}_N = \boldsymbol{\Sigma}_N \left( \boldsymbol{\Sigma}_0^{-1} \boldsymbol{\mu}_0 + \sigma^{-2} \boldsymbol{\Phi}^\top \mathbf{y} \right), \quad (19)$$

$$\boldsymbol{\Sigma}_N = \left( \sigma^{-2} \boldsymbol{\Phi}^\top \boldsymbol{\Phi} + \boldsymbol{\Sigma}_0^{-1} \right)^{-1}. \quad (20)$$

We are interested in the predictive uncertainty for a new test point  $(\mathbf{x}_*, y_*)$  so we inspect the predictive posterior and its properties:

$$\begin{aligned} p(y_*|\mathbf{x}_*, \mathbf{y}, \mathbf{X}) &= \int p(y_*|\mathbf{x}_*, \boldsymbol{\theta}) p(\boldsymbol{\theta}|\mathbf{y}, \mathbf{X}) d\boldsymbol{\theta} \\ &= \mathcal{N}(y_*|\boldsymbol{\mu}_N^\top \boldsymbol{\phi}(\mathbf{x}_*), \underbrace{\sigma^2 + \boldsymbol{\phi}(\mathbf{x}_*)^\top \boldsymbol{\Sigma}_N \boldsymbol{\phi}(\mathbf{x}_*)}_{\mathbb{V}[y_*|\mathbf{x}_*, \mathbf{y}]}) \end{aligned} \quad (21)$$

where  $\boldsymbol{\mu}_N$  and  $\boldsymbol{\Sigma}_N$  are the posterior mean and covariance matrix. From the predictive variance  $\mathbb{V}[y_*|\mathbf{x}_*, \mathbf{y}]$  we identify two components: (i)  $\sigma^2$  which represents the uncertainty related to the data noise (AU) and (ii)  $\boldsymbol{\phi}(\mathbf{x}_*)^\top \boldsymbol{\Sigma}_N \boldsymbol{\phi}(\mathbf{x}_*)$  which is the uncertainty associated with model parameters (EU). As we discuss in Section 5.1, by defining  $\mathbb{V}[y_*|\mathbf{x}_*, \mathbf{y}] := \sigma_N^2(\mathbf{x})$  as the predictive uncertainty

for a new test point  $\mathbf{x}$  when training on  $N$  input points, we have that  $\sigma_{N+1}^2(\mathbf{x}) \leq \sigma_N^2(\mathbf{x})$ , meaning that the posterior distribution becomes narrower as additional data points are observed (Qazaz et al., 1997). Moreover,  $\lim_{N \rightarrow \infty} \sigma_N^2(\mathbf{x}) = \sigma^2$ ; that is, in the infinite data regime, the predictive uncertainty converges to its irreducible component, AU.

### A.1.1 From posterior predictive variance to Total Uncertainty

We now derive an expression for the (total) predictive uncertainty associated with a new data point  $(\mathbf{x}, y)$ , defined as the entropy of the predictive posterior:

$$\begin{aligned}
\text{TU}(\mathbf{x}) &= \mathbb{H}[p(y|\mathbf{x}, \mathbf{y}, \mathbf{X})] \\
&= \frac{1}{2} \log(2\pi e \sigma_N^2(\mathbf{x})) \\
&= \frac{1}{2} \log \left( 2\pi e \left( \sigma^2 + \phi(\mathbf{x})^\top \left( \sigma^{-2} \Phi^\top \Phi + \Sigma_0^{-1} \right)^{-1} \phi(\mathbf{x}) \right) \right) \\
&= \frac{1}{2} \log \left( 2\pi e \sigma^2 \left( 1 + \sigma^{-2} \phi(\mathbf{x})^\top \left( \sigma^{-2} \Phi^\top \Phi + \Sigma_0^{-1} \right)^{-1} \phi(\mathbf{x}) \right) \right) \\
&= \frac{1}{2} \log(2\pi e \sigma^2) + \frac{1}{2} \log \left( 1 + \sigma^{-2} \phi(\mathbf{x})^\top \left( \sigma^{-2} \Phi^\top \Phi + \Sigma_0^{-1} \right)^{-1} \phi(\mathbf{x}) \right) \\
&= \underbrace{\frac{1}{2} \log(2\pi e \sigma^2)}_{\text{AU}(\mathbf{x})} + \underbrace{\frac{1}{2N} \phi(\mathbf{x})^\top \Sigma_\phi^{-1} \phi(\mathbf{x})}_{\text{EU}(\mathbf{x})} + O\left(\frac{1}{N^2}\right)
\end{aligned} \tag{22}$$

In the previous derivation, we assume  $\mathbf{X} = (\mathbf{x}_1, \dots, \mathbf{x}_N)$  to be a collection of IID samples with  $\mathbf{0}$  mean and  $\Sigma_x$  covariance matrix. The same holds for  $\Phi$  where samples  $\phi(\mathbf{x})$  are drawn independently from a distribution with  $\mathbf{0}$  mean and  $\Sigma_\phi$  covariance matrix. By the Law of Large Numbers  $\frac{1}{N} \Phi^\top \Phi \rightarrow \mathbb{E}[\phi(\mathbf{x})\phi(\mathbf{x})^\top] = \Sigma_\phi$  as  $N \rightarrow \infty$  which implies  $\Phi^\top \Phi \rightarrow N\Sigma_\phi$ . In addition, for large  $N$  the  $\Sigma_0^{-1}$  term vanishes. This shows that as  $N \rightarrow \infty$ , TU approaches AU and the EU decays with rate  $\frac{1}{N}$ .

## A.2 Total Uncertainty and Generalization Error for linear models

In this Section we formally derive a connection between the Watanabe generalization error  $G_N$  and the Total Uncertainty (TU) for Bayesian linear models. Using the notation from Watanabe (2009, 2018) the generalization error  $G_N$  and the Free Energy  $F_N$  are defined as:

$$G_N = \mathbb{E}_{p(y_{N+1}|\mathbf{x}_{N+1}, \boldsymbol{\theta}_{\text{true}})}[F_{N+1}] - F_N \tag{23}$$

$$F_N = -\log p(\mathbf{y}_N|\mathbf{X}_N) = -\log \int p(\mathbf{y}_N|\mathbf{X}_N, \boldsymbol{\theta}) p(\boldsymbol{\theta}) d\boldsymbol{\theta}. \tag{24}$$

We consider the same linear model of Appendix A.1 and without loss of generality we set the basis functions to be identity functions, i.e.,  $\phi(\mathbf{x}) = \mathbf{x}$ . We also introduce  $\boldsymbol{\theta}_{\text{true}}$ , the set of underlying true parameters. A new data point  $(\mathbf{x}_{N+1}, y_{N+1})$  is generated according to the true process:

$$y_{N+1} \sim \mathcal{N}(y_{N+1}|\mathbf{x}_{N+1}, \boldsymbol{\theta}_{\text{true}}) = \mathcal{N}(y_{N+1}|\boldsymbol{\theta}_{\text{true}}^\top \mathbf{x}_{N+1}, \sigma_{\text{true}}^2). \tag{25}$$

The free energy  $F_N$  is defined as the negative log marginal likelihood:

$$\begin{aligned}
F_N &= -\log p(\mathbf{y}_N|\mathbf{X}_N) \\
&= -\log \int p(\mathbf{y}_N|\mathbf{X}_N, \boldsymbol{\theta}) p(\boldsymbol{\theta}) d\boldsymbol{\theta} \\
&= -\log \int \left( \prod_{n=1}^N p(y_n|\mathbf{x}_n, \boldsymbol{\theta}) \right) p(\boldsymbol{\theta}) d\boldsymbol{\theta}.
\end{aligned} \tag{26}$$

We now relate  $F_{N+1}$  and  $F_N$ , the free energy for  $N+1$  and  $N$  input points, respectively:

$$\begin{aligned}
F_{N+1} &= -\log p(Y_{N+1}|\mathbf{X}_{N+1}) \\
&= -\log p(y_{N+1}, \mathbf{y}_N|\mathbf{x}_{N+1}, \mathbf{X}_N) \\
&= -\log p(y_{N+1}|\mathbf{x}_{N+1}, D_N)p(\mathbf{y}_N|\mathbf{X}_N) \\
&= -\log p(y_{N+1}|\mathbf{x}_{N+1}, D_N) - \log p(\mathbf{y}_N|\mathbf{X}_N) \\
&= -\log p(y_{N+1}|\mathbf{x}_{N+1}, D_N) + F_N
\end{aligned} \tag{27}$$

where  $D_N = \{\mathbf{X}_N, \mathbf{y}_N\}$  and  $p(y_{N+1}|\mathbf{x}_{N+1}, D_N)$  is the posterior predictive distribution for the  $(N+1)$  data point given the first  $N$  data points:

$$\begin{aligned}
p(y_{N+1}|\mathbf{x}_{N+1}, D_N) &= \int p(y_{N+1}|\mathbf{x}_{N+1}, \boldsymbol{\theta})p(\boldsymbol{\theta}|D_N)d\boldsymbol{\theta} \\
&= \mathcal{N}(y_{N+1}|\mu_{\text{pred}}, \sigma_{\text{pred}}^2),
\end{aligned} \tag{28}$$

$$\mu_{\text{pred}} := \mathbb{E}[y_{N+1}|\mathbf{x}_{N+1}, D_N] = \boldsymbol{\mu}_N^\top \mathbf{x}_{N+1} \tag{29}$$

$$\sigma_{\text{pred}}^2 := \mathbb{V}[y_{N+1}|\mathbf{x}_{N+1}, D_N] = \sigma_{\text{true}}^2 + \mathbf{x}_{N+1}^\top \boldsymbol{\Sigma}_N \mathbf{x}_{N+1}. \tag{30}$$

Let's simplify the notation: we rename the new data point  $y_{N+1}$  simply  $y$  such that  $p(y) := p(y_{N+1}|\mu_{\text{true}}, \sigma_{\text{true}}^2)$  where  $\mu_{\text{true}} := \boldsymbol{\theta}_{\text{true}}^\top \mathbf{x}_{N+1}$ . We can now compute the generalization error:

$$\begin{aligned}
G_N &= \mathbb{E}_{p(y)}[F_{N+1}] - F_N \\
&= \mathbb{E}_{p(y)}[F_{N+1} - F_N] \\
&= \mathbb{E}_{p(y)}[-\log p(y_{N+1}|\mathbf{x}_{N+1}, D_N)] \\
&= \mathbb{E}_{p(y)} \left[ \frac{1}{2} \log(2\pi\sigma_{\text{pred}}^2) + \frac{(y - \mu_{\text{pred}})^2}{2\sigma_{\text{pred}}^2} \right] \\
&= \frac{1}{2} \log(2\pi\sigma_{\text{pred}}^2) + \frac{\sigma_{\text{true}}^2 + (\mu_{\text{true}} - \mu_{\text{pred}})^2}{2\sigma_{\text{pred}}^2} \\
&= \underbrace{\mathbb{H}[\mathcal{N}(y|\mu_{\text{true}}, \sigma_{\text{true}}^2)]}_{\text{AU}(\mathbf{x}_{N+1})} + \underbrace{\text{KL}[\mathcal{N}(y|\mu_{\text{true}}, \sigma_{\text{true}}^2) || \mathcal{N}(y|\mu_{\text{pred}}, \sigma_{\text{pred}}^2)]}_{\text{EU}(\mathbf{x}_{N+1})} \tag{31}
\end{aligned}$$

where we used the fact that  $\mathbb{E}_{p(y)}[(y - \mu_{\text{pred}})^2] = \mathbb{V}_{p(y)}[y] + (\mu_{\text{true}} - \mu_{\text{pred}})^2 = \sigma_{\text{true}}^2 + (\mu_{\text{true}} - \mu_{\text{pred}})^2$  and:

$$\mathbb{H}[\mathcal{N}(y|\mu_{\text{true}}, \sigma_{\text{true}}^2)] = \frac{1}{2} \log(2\pi e \sigma_{\text{true}}^2) \tag{32}$$

$$\text{KL}[\mathcal{N}(y|\mu_{\text{true}}, \sigma_{\text{true}}^2) || \mathcal{N}(y|\mu_{\text{pred}}, \sigma_{\text{pred}}^2)] = \frac{1}{2} \log \left( \frac{\sigma_{\text{pred}}^2}{\sigma_{\text{true}}^2} \right) + \frac{\sigma_{\text{true}}^2 + (\mu_{\text{true}} - \mu_{\text{pred}})^2}{2\sigma_{\text{pred}}^2} - \frac{1}{2}. \tag{33}$$

This is closely related to the asymptotic expression we derived for TU in [Appendix A.1.1](#) where, if we now consider identity basis functions and a test point  $\mathbf{x}_{N+1}$ , it becomes:

$$\text{TU}(\mathbf{x}_{N+1}) = \underbrace{\frac{1}{2} \log(2\pi e \sigma_{\text{true}}^2)}_{\text{AU}(\mathbf{x}_{N+1})} + \underbrace{\frac{1}{2(N+1)} \mathbf{x}_{N+1}^\top \boldsymbol{\Sigma}_N^{-1} \mathbf{x}_{N+1}}_{\text{EU}(\mathbf{x}_{N+1})} + O\left(\frac{1}{(N+1)^2}\right) \tag{34}$$

In terms of generalization error  $G_N$ , as the posterior predictive  $q_N(y)$  moves closer to the true data generating distribution  $p(y)$ , the KL term goes to zero and  $G_N$  converges to the aleatoric component  $\frac{1}{2} \log(2\pi e \sigma_{\text{true}}^2)$ , i.e., if  $\mu_{\text{pred}} = \mu_{\text{true}}$  and  $\sigma_{\text{pred}}^2 = \sigma_{\text{true}}^2$  then  $\text{KL} [\mathcal{N}(y|\mu_{\text{true}}, \sigma_{\text{true}}^2) || \mathcal{N}(y|\mu_{\text{pred}}, \sigma_{\text{pred}}^2)] = 0$ .

### A.2.1 Asymptotic behaviors

In [Watanabe \(1999\)](#); [Hayashi and Sawada \(2025\)](#) it's showed that the generalization error and the free energy have the asymptotic expansion:

$$\mathbb{E}_n[G_N] = \frac{\lambda}{n} - \frac{m-1}{n \log n} + o\left(\frac{1}{n \log n}\right) \quad (35)$$

$$F_N = nS_n + \lambda \log n - (m-1) \log \log n + O_p(1) \quad (36)$$

where  $\lambda$  is a positive rational number,  $m$  a positive integer and  $\mathbb{E}_n[\cdot]$  is the expectation operator the overall dataset. The constant  $\lambda$  is called a learning coefficient since it is dominant in the leading terms of the equations above, which represents the  $\mathbb{E}_n[G_n] - n$  and  $F_n - n$  learning curves.  $m$  is called a multiplicity in algebraic geometry. In the case of regular models  $\lambda = \frac{d}{2}$  and  $m = 1$  where  $d$  is the number of model parameters.

## B Additional results

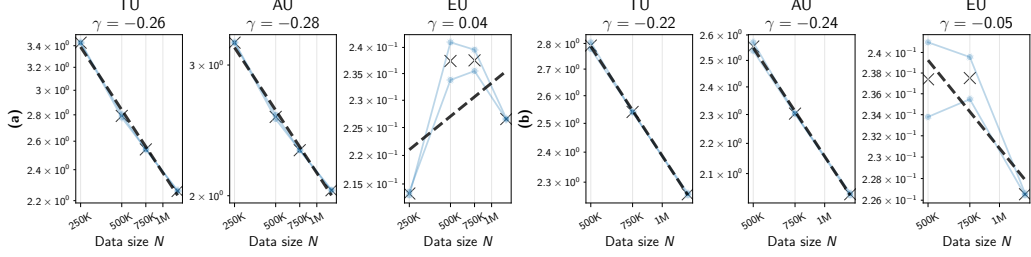


Figure 9: **Vision Transformer (ViT) on ImageNet-32 dataset:** We use MC dropout with fixed dropout rate  $p = 0.1$ . We train for 200 epochs using SGD with cosine annealing. In **(a)** we report uncertainty scaling on subsets from size 250K up to 1.2M. In **(b)** we discard the first point highlighting the decreasing rate of EU for large values of  $N$ .

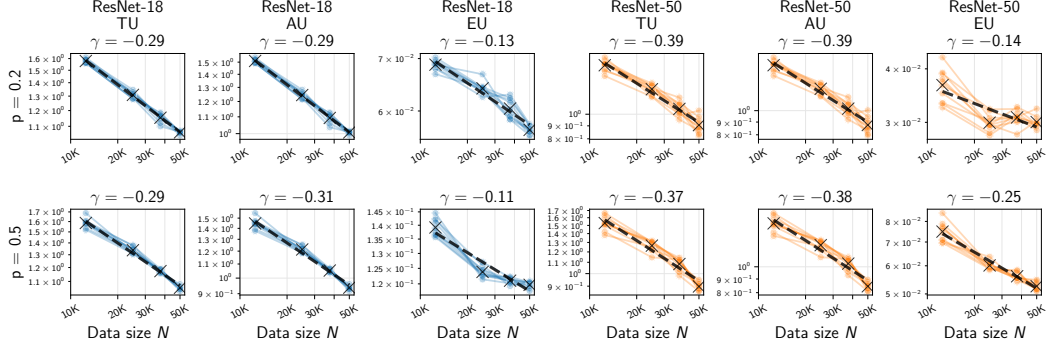


Figure 10: **ResNets on CIFAR-100 dataset:** We train the models with MC dropout with fixed dropout rate  $p = 0.2$  (*first row*) and  $p = 0.5$  (*second row*). We consider 25%, 50%, 75% and 100% subsets of the training data. We report results from 10 independent folds (varying both data subsampling and model initialization) showing the mean uncertainty for each  $N$  subset. The dashed lines represent linear regressions fitted to the average (over the folds for every  $N$ ) of each uncertainty metric. Both axes are on a logarithmic scale.

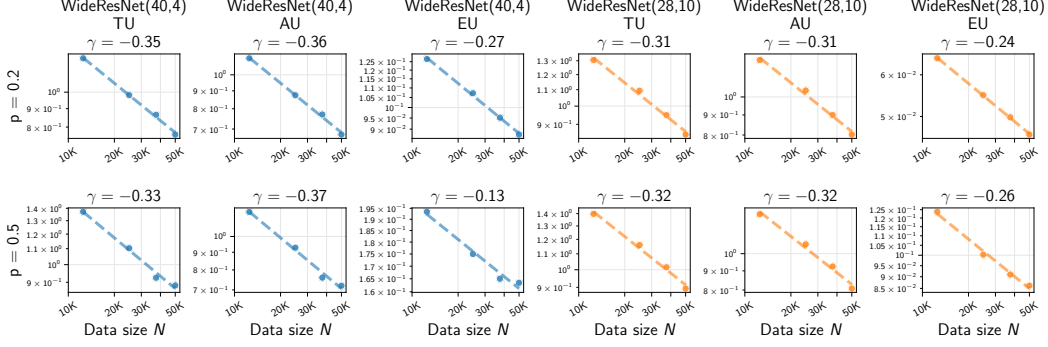


Figure 11: **WideResNets on CIFAR-100 dataset:** We train the models with MC dropout with fixed dropout rate  $p = 0.2$  (*first row*) and  $p = 0.5$  (*second row*). We consider 25%, 50%, 75% and 100% subsets of the training data and we show the mean uncertainty for each  $N$  subset. Dashed lines represent linear regression fitted to the test mean of each uncertainty metric. Both axes are on a logarithmic scale.

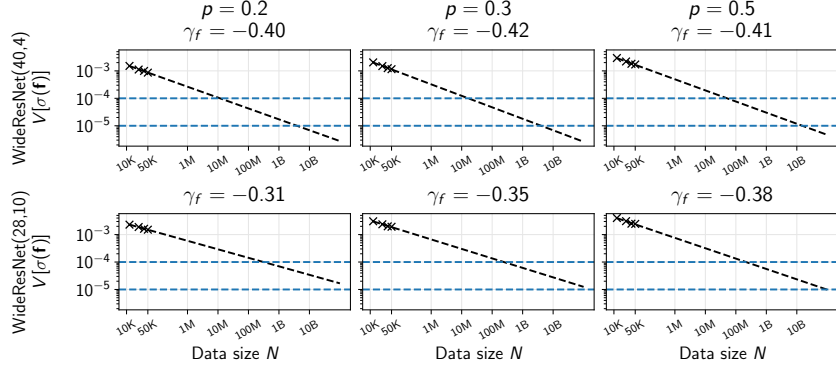


Figure 12: **WideResNets on CIFAR-10 dataset - extrapolation:** We report uncertainty trends for different WideResNets and dropout rates. We mention in the main paper that the scaling laws we derive in this context are practically useful to extrapolate uncertainties to  $N$  arbitrarily large. We report  $\mathbb{V}[\sigma(\mathbf{f})]$ , the variance computed over the Softmax predictions of the MC samples, averaged over all the test samples ( $\times$  in the plots). The black dashed lines have slope  $\gamma_f$ , the blue dashed lines correspond to two thresholds of predictive uncertainty.

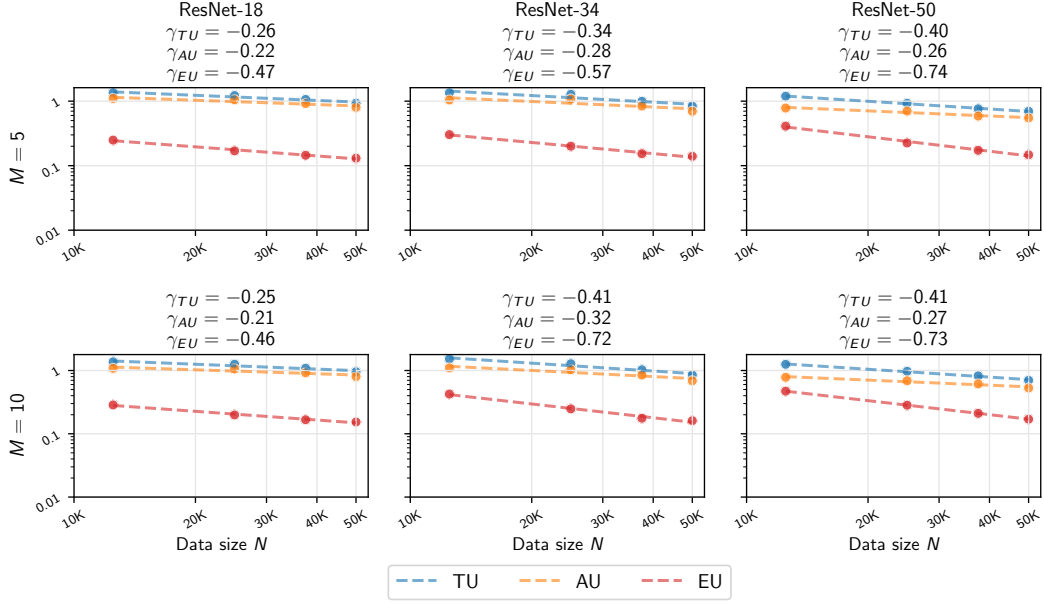


Figure 13: **ResNets on CIFAR-100 dataset with Deep Ensembles:** We train the models with Deep Ensembles with ensemble members  $M = 5$  (*first row*) and  $M = 10$  (*second row*). We consider 25%, 50%, 75% and 100% subsets of the training data and we show the mean uncertainty for each  $N$  subset. Dashed lines represent linear regression fitted to the test mean of each uncertainty metric. Both axes are shown on a logarithmic scale.

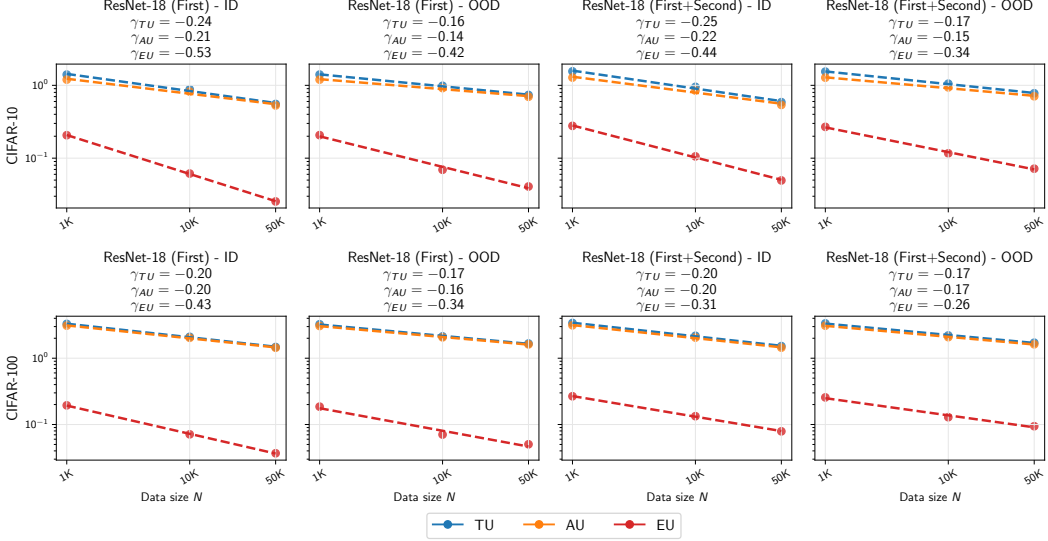


Figure 14: **ResNet-18 on CIFAR-10 and CIFAR-100 datasets with MCMC:** We report uncertainties obtained through MCMC considering only the first layer stochastic (First) and only the first two layers stochastic (First+Second). We show the scaling for both in-distribution (ID) and out-of-distribution (OOD) predictive uncertainties. On the first row the mean uncertainty scaling for CIFAR-10 using CIFAR-10-C as OOD dataset while on the second row the mean uncertainty scaling for CIFAR-100 using CIFAR-100-C as OOD dataset.

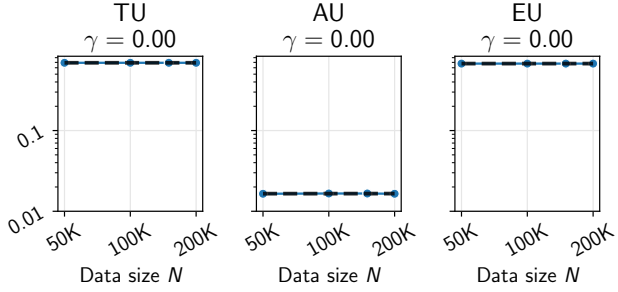


Figure 15: **Uncertainty scaling with Bayesian LoRA:** For completeness, we report the uncertainty scaling we get when fine-tuning LLM Phi on Quora Questions Pairs (qqp) dataset using increasing training subsets and by doing Laplace approximation over the LoRA parameters following Yang et al. (2024). These curves are completely flat, suggesting that assessing predictive uncertainty on much smaller (fine-tuning) data compared to the massive amount used for pre-training doesn't give any insight about the scaling laws of the metrics of interest.

## C Experimental setup

Table 1: Vision Transformer (ViT) architecture - implementation from <https://github.com/kentaroy47/vision-transformers-cifar10>.

Parameter	Value
Patch size	4
Embedding dimension	512
Transformer depth	6
Number of attention heads	8
MLP hidden dimension	256
Dropout (transformer)	{0.1, 0.5}
Dropout (embeddings)	{0.1, 0.5}

Table 2: **Algorithmic dataset**: To obtain the results in Fig. 4 we use a GPT-2 and train it for 10.000 epochs with AdamW optimizer (learning rate  $10^{-4}$ ) and linear scheduler with 100 warmup steps - implementation from <https://github.com/openai/grok/tree/main/scripts>.

Parameter	Value
Max sequence length	256
Embedding size	128
Number of layers	2
Number of attention heads	4
Dropout (residuals)	0.1
Dropout (embeddings)	0.1
Dropout (attention)	0.1